Mem. S.A.It. Vol. 76, 735

**Memorie** della


# Solar spectral irradiance variability comparisons of the SORCE SIM instrument with monitors of solar activity and spectral synthesis

J. Harder, J. Fontenla, O. White, G. Rottman and T. Woods

Laboratory for Atmospheric and Space Physics (LASP), University of Colorado, 1234 Innovation Drive, Boulder, CO 80303
e-mail: jerald.harder@lasp.colorado.edu

**Abstract.** The SORCE (Solar Radiation and Climate Experiment) SIM (Spectral Irradiance Monitor) instrument is a satellite-borne prism spectrometer that measures the solar spectrum from 200-2700 nm with a cadence of at least 2 spectra per day with a resolution of 1-33 nm. The nearly 800-day long data set provides the temporal evolution of solar irradiance throughout ultraviolet, visible and infrared spectral regions. At some wavelengths in the ultraviolet, the SIM measurements exhibit variations similar to Mg II index, and in the visible and IR they show similarities to Total Solar Irradiance (TSI) record, but with differing amplitudes, phases, and shapes relative to the monitors. The TSI can be explained as a complex mix of the various wavelength components observed by SIM. Further insight into the solar variability observed by SIM can be gained from comparing an analysis of the distribution of solar features as measured by PSPT (Precision Solar Photometric Telescope) in conjunction with spectral synthesis. Most of the observed behavior appears to be qualitatively explained by the observed solar surface features that directly relate to the magnetic activity but some IR variations are not readily explained as was noted by Fontenla et al. (2004).

**Key words.** spectral irradiance – solar variabilty

## 1. Introduction

The Spectral Irradiance Monitor (SIM) was developed to replace and extend the UARS SOLSTICE n-channel spectrometer (Rottman et al. , 1993) that was used to study solar variability in the 280-430 nm region. The SIM instrument covers a much wider spectral range (200-2700 nm) and uses an electrical substitution radiometer (ESR) as its primary detector. A Fèry prism is used in place of a grating so the instrument can be used over the full wavelength range with only one optical element thereby simplifying the spectrometer design and operation.

A comprehensive account of the design and operating principal of the SIM spectrometer and the ESR detector has been presented previously (Harder et al. , 2005a,b), but will be summarized here. The SIM instrument consists of two mirror image spectrometers packaged in a single housing; one spectrometer is used for daily measurements while the other is used for

*Send offprint requests to*: J. Harder

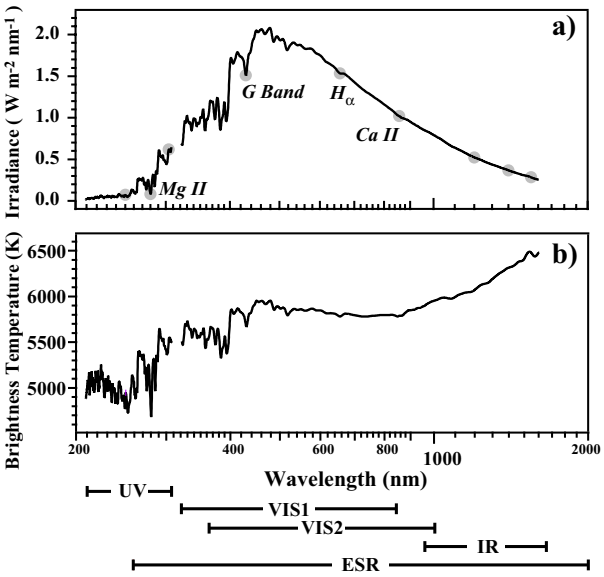


**Fig. 1.** Irradiance (panel a) and brightness temperature (panel b) spectra measured by SIM. Graph shows as gray dots selected wavelengths that will be discussed in subsequent sections of the paper. The bars at the bottom identify the detectors and their useful operating ranges.

monthly comparative studies. These two spectrometers are coupled by a periscope system for tracking each spectrometers prism transmission degradation by using one spectrometer as a monochromator for the other. The spectrometer has a wavelength dependent resolution that is proportional to the dispersion of the prism glass (i.e. the first derivative of the index of refraction with respect to $\lambda$). The spectrometers resolving power ($\lambda/\Delta\lambda$) varies from 378 nm at 250 nm, to a minimum of 37 nm at 1260 nm, and increases slowly in the infrared to 142 nm at 2700 nm. A suite of 5 independent detectors is used to allow efficient coverage of the instruments wide spectral band. Three silicon photodiodes are used for the UV-Visible region, InGaAs for near infrared, and the ESR is used throughout the spectrum (260 to 2700 nm). The ESR is used to calibrate the radiant sensitivity of the photodiodes by making a comparative measurement at 50 selected wavelengths that are tracked on a daily basis throughout the mission. The full solar spectrum is measured only every three months with the ESR as the main detector since long integration times are needed at each prism step. Figure 1 shows the spectrum measured by the four photodiodes. Panel a) is the irradiance spectrum, and panel b) is the equivalent brightness temperature spectrum. Also shown on the graph are the operating ranges for each of these detectors and the spectra in this figure are composite of the four photodiode detectors.

SIM measures 2 absolute irradiance spectra per day, and time series can be constructed from these spectra at any given wavelength. In this paper, we will discuss the time series from 21 April 2004 to 01 June 2005, which represents a time period of stable operations during the mission. The wavelengths of the time series discussed in this paper are marked on panel a) of Figure 1 with gray dots.

## 2. Time series of solar variability as measured by SIM and comparisons with Mg II and TSI

The 21 April 2004  1 June 2005 is a time period of declining activity for Solar Cycle 23 and covers about 15 solar rotation periods. However, during this time period there was still marked chromospheric solar activity as

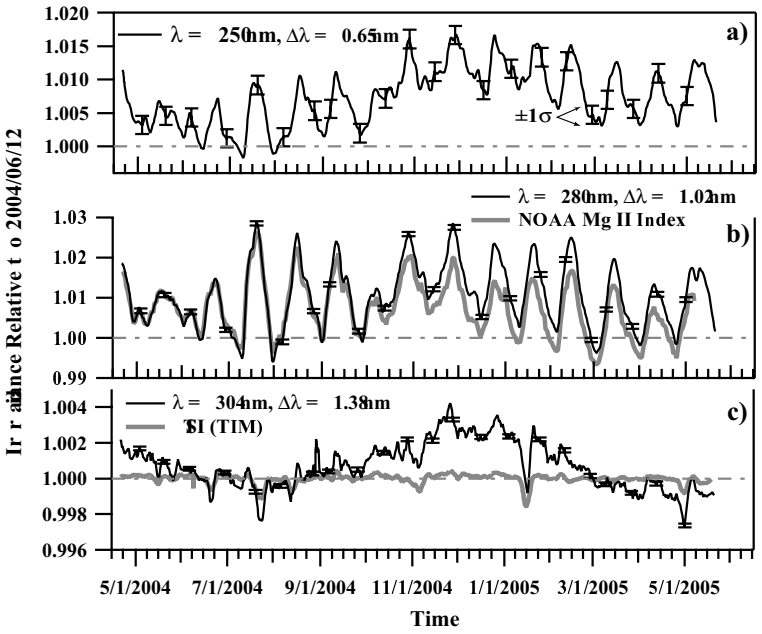


**Fig. 2.** Relative irradiance time series in the ultraviolet part of the spectrum at 250 nm, 280 nm (Mg II), and 304 nm. The relative irradiance is found from the ratio the daily irradiance to that of 12 June 2004, a day of low solar activity. Each panel of the graph shows the wavelength and the instrument resolution and estimates of the $\pm 1\sigma$ measurement precision. Figure 2b has the relative NOAA Mg II index over-plotted for comparison and Figure 2c over-plots the relative TSI.

measured by the NOAA Mg II index (Viereck and Puga , 1999; Kopp et al. , 2005) (and www.sec.noaa.gov/ftpmenu/sbuv.html), and the passage of a number of significant sunspots (Kopp et al. , 2005). Furthermore, the levels of solar activity can be deduced from analysis of solar images such as those from the Precision Solar Photometric Telescope (herein called PSPT, see http://rise.hao.ucar.edu/). Because solar irradiance has not yet reached minimum levels, the best way to compare irradiance variations is to select a reference day, and ratio the daily spectra to this value. The reference day for subsequent graphs in this paper is 12 June 2004; this day was selected to give the same scaling shown in (Rottman et al. , 2005). Figure 2 shows the time series of relative solar spectral irradiance in the ultraviolet part of the spectrum. Each panel of this figure shows the wavelength and the instrument resolution, as defined by the full width half maximum of the nearly triangular instrument function. The recorded irradiance is then the solar spectrum weighted over this bandpass. Each graph also shows the $\pm 1\sigma$ estimated precision of the SIM measurement. Panel a) shows the time series at 250 nm, panel b) is at 280 nm along with the NOAA Mg II index, and panel c) shows the 304 nm time series along with the relative TSI measurement. At 250 nm (Figure 2a), the irradiance signal is composed of a mixture of continuum formed near the top of the photosphere combined with many deep absorption lines formed in the lower chromosphere. Although variability at this wavelength is a mixture of these two contributions, the variability is dominated by the chromospheric line component and shows similarities to the Mg II index variations. The photospheric continuum tends to decrease in brightness due to the presence of sunspots (similar to TSI), but the chromospheric line component increases due to the presence of plage.

Figure 2b shows the irradiance at 280 nm, and this measurement includes the line cores of both Mg II h and k lines, their line wings, and a pseudo-continuum. This pseudo-continuum has the same characteristics discussed for the 250 nm band, however, the line cores have a very strong upper chromospheric signature because these emission features show large intensity increases in active regions. Because of this,, the variability at this wavelength is large and is chromospheric in character with the irradiance peaking when plage areas are largest and also coincides with times near the TSI minima when the sunspot areas reach a maximum value. Figure 2b shows SIM 280 nm irradiance tracking the NOAA Mg II index with similar amplitudes. This level of agreement is mostly due to the fact that SIM and NOAA SBUV instruments have similar spectral resolutions. Active network causes a trend difference between the SIM 280 nm irradiance and the Mg II index because of common mode suppression of irradiance changes in the wings of the Mg II absorption feature.

The SIM irradiance in the 304 nm band (Figure 2c) is also a pseudo-continuum. The continuum at this wavelength is produced slightly deeper in the photosphere, and the distribution of absorption lines is less dense than at 250 nm. As a result, the behavior is more photospheric, less chromospheric, and appearance of sunspot passages is now present in the time series. The time series now resembles the TSI but with larger variations, and the the presence of active network contributes to increased irradiance level. Figure 2c shows spectral irradiance decreases on the order of 0.2% with the passage of sunspots while the TSI decreased by only about half as much.

Figure 3 is analogous to Figure 2 but for three spectral bands in the visible. Figure 3a is the band centered at 430 nm and corresponds to the G-band that appears as a prominent absorption feature in the SIM data (see Figure 1). It consists of many dense, narrow molecular lines (predominately CH), several very deep resonance Fe I lines, and the H Balmer gamma line at 434.25 nm. The molecular lines originate in the upper photosphere and low chromosphere, and they are deeper in sunspots where the sunspot continuum is also depressed. The behavior of this band is similar to that of the TSI except that the sunspot minima are deeper by about factor of 1.5. The irradiance increases due to faculae near the limb, and network structure still contributes to the irradiance at this wavelength. Figure 3b and 3c shows the time series for the wavelengths 656 nm and 857 nm where the broad and deep H Balmer alpha line and the Ca II IR triplet lines are the dominant spectral features. However, due to the large bandwidth of the SIM instrument at these wavelengths, the contributions from the continuum outside of these spectral lines dominate. This is seen in Figure 1 where only very weak absorption features are evident in the SIM spectrum at these locations. The relative irradiance variation in the 656 nm band (Figure 3b) is almost identical to the TSI relative variations, particularly in the amplitude of the variations associated with sunspot, faculae, and plage. Figure 3c shows variability in the 857 nm band which is also similar to TSI except that the observed sunspot contrast is now smaller.

Figure 4 shows the relative variation of the irradiance in the 1200, 1400, and 1590 nm bands. At these wavelengths, the data indicates the disappearance of irradiance enhancements due to faculae near the limb that is common in the visible wavelengths (see Figure 3). This effect is apparent in these plots where the TSI irradiance variations exceeds those of the spectral irradiance, and this is attributed to plage and active network brightness enhancements at the visible wavelengths, but not at the IR wavelengths shown in this figure. This figure also shows the expected reduction in sunspots contrast relative to the TSI, and this contrast reduction is wavelength dependent with lower contrast at longer wavelengths. Multiple infrared enhancements features that correspond to an enhancement of about +120 ppm above the relative TSI level are apparent in all three panels of this figure (the enhancements are marked with arrows). These are similar features to the ones described by Fontenla et al. (2004). In particular, during the February to June 2005 time frame, these features are not observed at

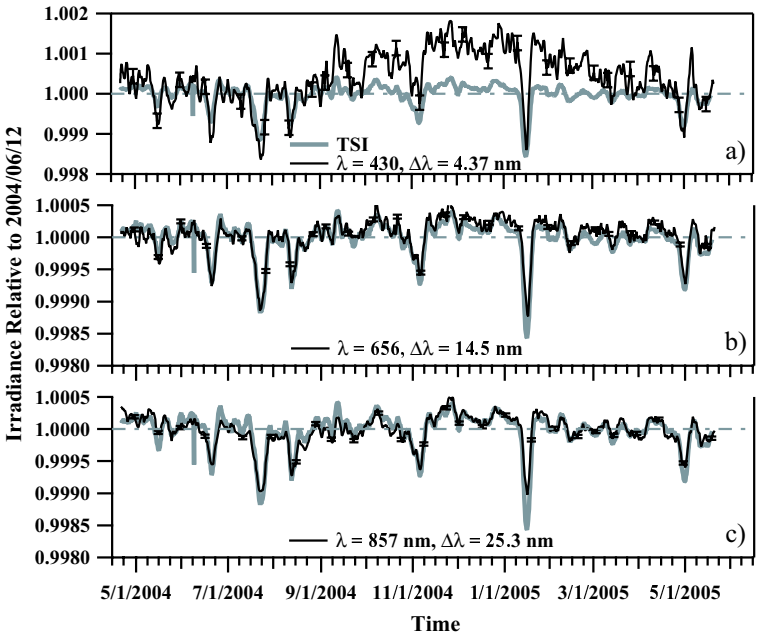


**Fig. 3.** Relative irradiance time series in the visible part of the spectrum: panel a) the G-band, panel b) near H$\alpha$, panel c) near Ca II infrared triplet.

wavelengths in the visible and UV. This may suggest that this infrared enhancement is due to a low-contrast structure deep in the solar photosphere; clearly more research is needed to understand and characterize this observation.

## 3. SIM and SRPM comparisons of solar variability

One of the lines of research that we are pursuing with the SIM instrument is to compare the time series provided by this instrument with findings from the SRPM model (Solar Radiation Physical Modeling) of solar irradiance synthesis (Fontenla et al. , 2005a,b). Following these two independent tracks allows us to address the following: 1) Evaluate the relative contributions and evolution of seven solar features (Fontenla et al. , 1999), 2) Verify the agreement between the SRPM method and SIM observations. This reveals, on one hand, places where further research is needed to improve the image analysis and models used by the SRPM method, and on the other hand, provides a strong constraint on how well the spectrometer is measuring solar irradiance; in particular, helping to separate long-term trends in solar variability from biases and slow drifts in the instrument calibration (Harder et al. , 2005b).

As currently implemented, the SRPM analysis method employs images acquired by the PSPT from Mauna Loa Observatory. This method combines the solar atmosphere models of temperature and density for solar surface structures, the radiative transfer computation of high-resolution spectra, and the areas and locations of the features needed to compute the solar spectral irradiance at a particular time. The analysis method can be briefly summarized as follows: 1) Seven solar surface structure types are identified and assigned the model atmospheres (Fontenla and Harder, 2005). Of particular importance to the current study, Fontenla et al. (2005a) define a penumbra model; previous comparative studies with SIM were limited due the absence of this key contribution. 2) The models are used

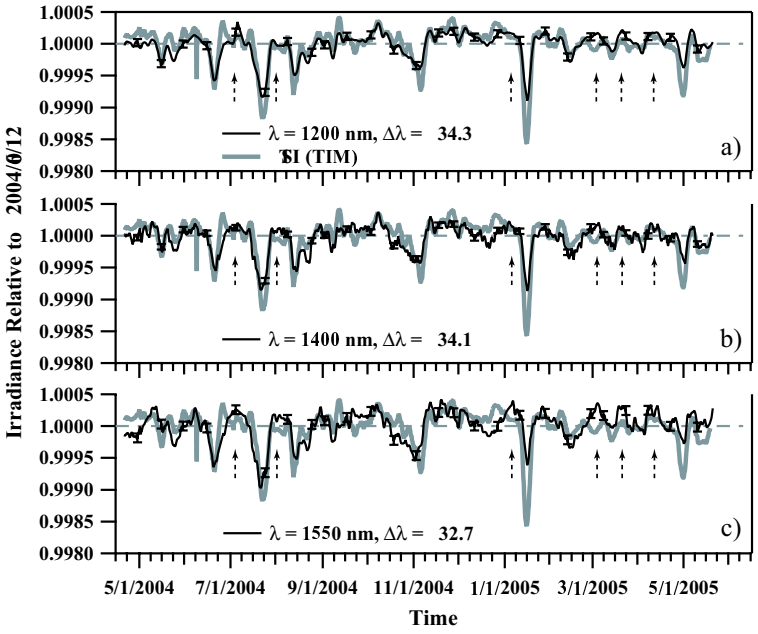


**Fig. 4.** Relative irradiance time series in the infrared part of the spectrum: panel a) 1200 nm, panel b) 1400 nm, panel c) 1550 nm, near the $H^-$ opacity minimum. The dashed arrows that appear in these three panels correspond to times when infrared enhancements similar to the ones discussed by Fontenla et al. (2004) appear in the time series.

to compute emergent intensity of each feature as a function of disk position. 3) Analyze Ca II (393.47±0.22 nm) and continuum (607.1± 0.23 nm) images to identify the seven solar surface features and determine their weighting according to area and position on the solar disk. 4) Calculate the irradiance on a specific day by combining intensities from each model atmosphere using results from the image analysis. 5) Convolve the high-resolution synthetic irradiance with the SIM spectral resolution function to obtain spectral estimates comparable to SIM measurements. At the present time these comparisons are limited to wavelengths between 400 and 1600 nm because of the current limitations of the spectral synthesis and the need for further analysis of SIM data out to 2.7 microns.

Figure 5 is analogous to Figure 3 but showing the SRPM calculation for five wavelengths in the visible and infrared spectral regions. Note also, that time range for this plot is from 01 October 2004 to 01 June 2005, covering a range of stable operations for the PSPT system at Mauna Loa. Figure 5a show the comparison at 430 in the neighborhood of the G-band, and a number of interesting features can be seen in this figure. 1) The calculated time series does not capture the contribution to active network. The PSPT images may not properly discriminate the features that constitute the active network, and this situation appears to be complicated by atmospheric turbulence. 2) Additional research is needed to model the chromospheric $T_{min}$, which defines the conditions where the molecular contributors to the G-band are the largest. 3) More work is also needed to account for not-LTE effects at the shorter wavelengths. The measured and modeled time series show better agreement at the longer wavelengths, as shown in Figures 5b and 5c for 656 nm and 857 nm, respectively. The improved agreement is predominately due to the inclusion of the penumbra model in the irradiance calculation. An interesting feature apparent in these two panels are the three sunspot passages

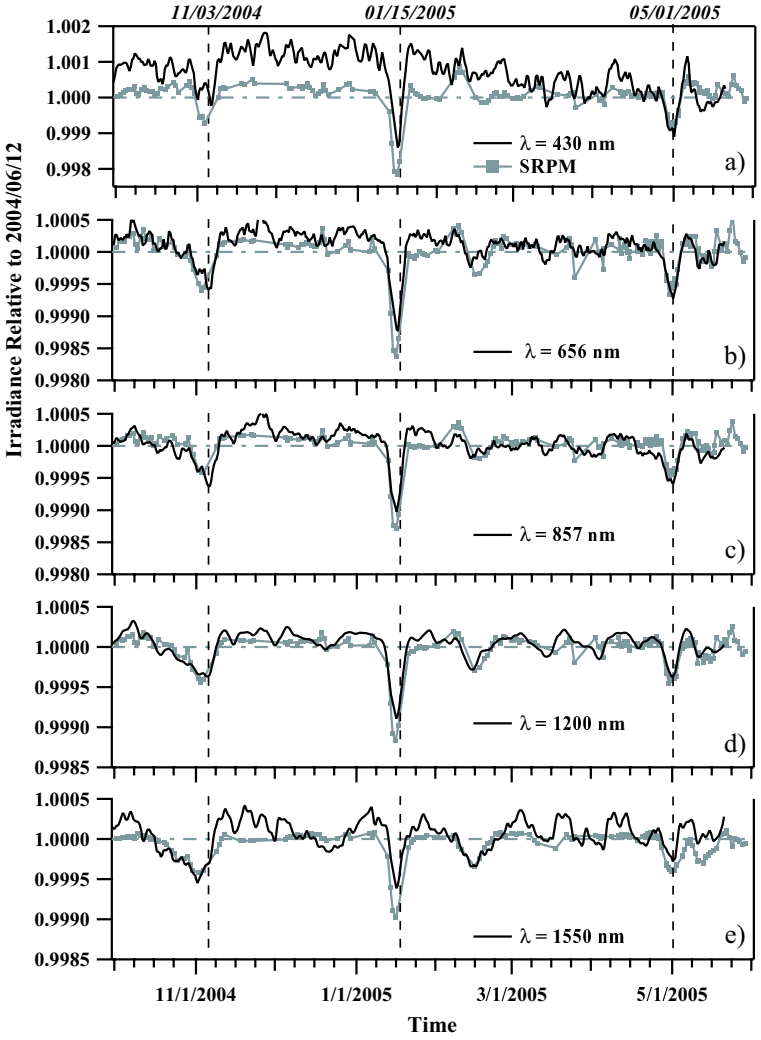


**Fig. 5.** Comparisons of relative SIM spectral irradiance to the SRPM calculation at the same wavelength. The dashed vertical lines correspond to times of sunspot passages discussed in the text.

during this time period (3 November 2004, 15 January 2005, and 1 May 2005) that show different levels of agreement between SIM and synthesis. This can be explained by the fact that Model S (sunspot model) used in the SRPM model is equivalent to the medium sunspot model discussed by Maltby et al. (1986). The 3 November 2004 and the 1 May 2005 sunspots are closely represented by Model S, but the 15 January 2005 sunspot is a shallow sunspot and has less contrast. Scattered light issues with ground-based solar imaging systems makes the discrimination of these shallow and deep sunspots difficult, but comparison of the SIM data with the current spectral synthesis will aid with their detection and analysis. Figures 5d and 5e show the SIM/SRPM comparison for 1200 nm, and 1550 nm. As in the visible measurements (see Figures 5b, and 5c), the inclusion penumbra model greatly improves the agreement in the infrared as well. Figures 5d and 5e also indicates that Model

S is adequate for the deep sunspots in the infrared, but some residual differences remain for the shallow sunspots. Figure 5e clearly shows that the current spectral synthesis does not address the excess irradiance seen in the infrared that requires further investigation.

## 4. Conclusions

This paper is a comparative study of the irradiance time series showing that the wavelength dependence of the observed solar spectral variations strongly depends on the contributions from sunspot umbra and penumbra, faculae, plage, and active network,and that each solar surface feature contributes differently throughout the solar spectrum. Since each type of surface feature evolves differently, the combination of their effects in integrated radiation over the entire solar disk produces the complicated variations seen in spectral irradiance time series and the TSI. The TSI and the Mg II index provide a strong constraint on the degree of solar activity, but the spectral variations observed by SIM at the wavelengths described in this study show important sources of variability, such as long-lived network structure in the UV and near-UV and facular brightening in the infrared, not directly addressed by these other activity monitors. Comparing the SIM spectral time series with SRPM solar feature models and the PSPT image analysis provides an additional dimension to the understanding to the sources of solar variations. The synthesis describes the evolution of solar surface features, and its contribution to the irradiance is in accord with the SIM observations. The level of agreement of the model with the observations provides a pathway to show where further research is needed to understand the sources of solar variability.

*Acknowledgements.* This work was supported by NASA contract NAS5-97045 at the University of Colorado.

## References

Fontenla, J. M., White, O. R., Fox, P. A., Avrett, E. H., & Kurucz, R. L. 1999, Astrophys. J., 518, 480

Fontenla, J. M., Harder, J., Rottman, G., Woods, T. N., Lawrence, G. M., & Davis, S. 2004, Astrophys. J. 605, L85

Fontenla, J. M., Averett, E., Thuillier, G., & Harder, J. 2005, submitted to Astrophys. J., June, 2005

Fontenla, J. M., & Harder, J., 2005, Mem. SAIt., this issue

Harder, J. W., Lawrence, G., Fontenla, J., Rottman, G., & Woods, T. 2005a, Solar Phys., in press

Harder, J., Fontenla, J., Lawrence, G., Rottman, G., & Woods, T. 2005b, Solar Phys., in press

Kopp, G., Lawrence, G., & Rottman, G. 2005, Solar Physics, in press

Maltby, P., Avrett, E., Carlsson, M., Kjeldseth-Moe, O., Kurucz, R., & Loeser, R. 1986, Astrophys. J., 306, 284

Rottman, G. J., T. Woods, & Sparn, T. 1993, J. Geophys. Res., 98, 10667

Rottman, G. J., Harder, J., Fontenla, J., Lawrence, G., & Woods, T. 2005, Solar Physics, in press

Viereck, R., & Puga, L. 1999, J. Geophys. Res., 104, 9995